Study of carbon nitride compounds synthesised by co-implantation of ^{13}C and ^{14}N in copper at different temperatures

Colaux, J.L.; Louette, P.; Colomer, J.-F.; Edmondson, P.D.; Donnelly, S.E.; Terwagne, G.

Published in:
Materials Chemistry and Physics

DOI:
10.1016/j.matchemphys.2010.11.016

Publication date:
2011

Document Version
Peer reviewed version

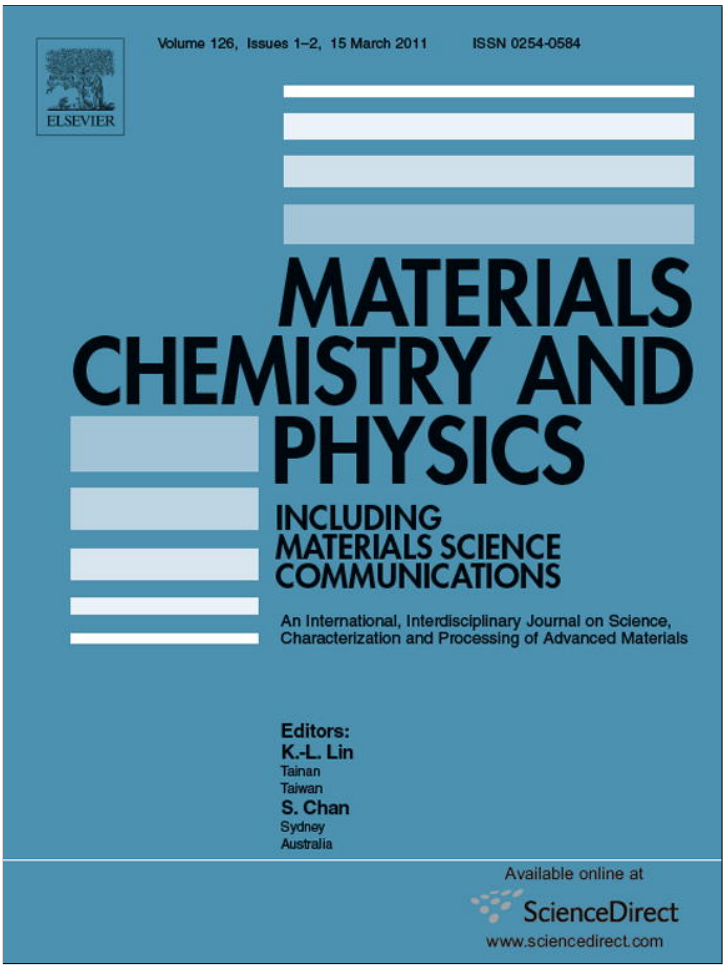

Materials Chemistry and Physics 126 (2011) 337–343

Contents lists available at ScienceDirect

Materials Chemistry and Physics

journal homepage: www.elsevier.com/locate/matchemphys

Study of carbon nitride compounds synthesised by co-implantation of ^{13}C and ^{14}N in copper at different temperatures

J.L. Colaux[a,*], P. Louette[b], J.-F. Colomer[c], P.D. Edmondson[d], S.E. Donnelly[d], G. Terwagne[a]

[a] LARN, Research Center in Physics of Matter and Radiation (PMR), University of Namur (FUNDP), 61 Rue de Bruxelles, 5000 Namur, Belgium
[b] LISE, Research Center in Physics of Matter and Radiation (PMR), University of Namur (FUNDP), 61 Rue de Bruxelles, 5000 Namur, Belgium
[c] LPS, Research Center in Physics of Matter and Radiation (PMR), University of Namur (FUNDP), 61 Rue de Bruxelles, 5000 Namur, Belgium
[d] Institute for Materials Research, University of Salford, Gtr. Manchester M5 4WT, UK

ARTICLE INFO

Article history:
Received 31 August 2009
Received in revised form 5 November 2010
Accepted 11 November 2010

Keywords:
Fullerenes
Nanostructures
Electron microscopy
XPS
Tribology

ABSTRACT

Carbon nitride compounds have been synthesised in copper by simultaneous high fluence (10^{18} at. cm^{-2}) implantation of ^{13}C and ^{14}N ions. During the implantation process, the substrate temperature was maintained at 25, 250, 350 or 450 °C. Depth profiles of ^{13}C and ^{14}N were determined using the non-resonant nuclear reactions (NRA) induced by a 1.05 MeV deuteron beam. The retained doses were deduced from NRA measurements and compared to the implanted fluence. The chemical bonds between carbon and nitrogen were studied as a function of depth and temperature by X-ray photoelectron spectroscopy (XPS). The curve fitting of C 1s and N 1s core level photoelectron spectra reveal different types of C–N bonds and show the signature of N_2 molecules. The presence of nitrogen gas bubbles in copper was highlighted by mass spectroscopy. The structure of carbon nitride compounds was characterised by transmission electron microscopy (TEM). For that purpose, cross-sectional samples were prepared using a focused ion beam (FIB) system. TEM observations showed the presence of small amorphous carbon nitride "nano-capsules" and large gas bubbles in copper. Based on our observations, we propose a model for the growth of these nano-objects. Finally, the mechanical properties of the implanted samples were investigated by nano-indentation.

1. Introduction

Since the prediction of its highly interesting physical properties in 1990 [1], the synthesis of the super-hard crystalline β-C_3N_4 phase has been extensively investigated. Although the fully crystalline phase has still not been reached, a wide variety of elaborate techniques such as reactive sputtering, chemical vapour deposition, pyrolysis of organic materials, laser deposition and ion implantation have been developed to synthesise this elusive carbon nitride structure [2–9]. Until now, this work has mainly focused on non-equilibrium synthesis conditions in order to prevent the formation of thermodynamically stable phases and reach the required 57 at.% of nitrogen to form the metastable β-C_3N_4 phase. However, despite pronounced non-equilibrium and energetic growth conditions, the nitrogen content in the resulting amorphous C_xN_y material rarely surpasses 30%. The nitrogen deficiency in the C_xN_y material seems to be due to the chemical desorption of volatile nitrogen-containing species from the growing film surface [10]. This phenomenon, first observed for ion beam assisted deposition [11], is predominant for all plasma-assisted techniques and limits the level of nitrogen incorporation [12]. The nitrogen deficiency in the C_xN_y material can also be due to the inherent drive of nitrogen to form strongly covalent bonded N_2 molecules, which then readily desorb [13].

In this work, the co-implantation of carbon and nitrogen in copper was used to synthesise the C_3N_4 like compounds. This process has some advantages compared to reactive sputtering. Indeed, the interaction between carbon and nitrogen atoms during the implantation process was enhanced due to their simultaneous arrival within the substrate, and their very low solubility inside copper favoured their precipitation into carbon nitride compounds. Moreover, the high compressive stresses applied by the matrix on the precipitates favoured compact growing structures [14,15]. Finally, the implantations were performed at medium energies (Table 1) so that the carbon and nitrogen atoms were buried from 200 to 900 nm in depth, preventing any chemical desorption of volatile nitrogen-containing species. Several implantations were then performed at 25, 250, 350 or 450 °C in order to study the influence of the temperature on the C_xN_y formation. The samples were fully characterised by NRA, XPS, TEM and nano-indentation methods in order to determine the carbon and nitrogen depth profiles, the C–N type bonds, the C_xN_y structures and the physical properties of the implanted areas, respectively.

* Corresponding author. Tel.: +32 81 72 54 79; fax: +32 81 72 54 74.
E-mail address: julien.colaux@fundp.ac.be (J.L. Colaux).

0254-0584/$ – see front matter © 2010 Elsevier B.V. All rights reserved.
doi:10.1016/j.matchemphys.2010.11.016

Table 1
Energies and calculated (R_{SRIM}) and experimental (R_{exp}) projected ranges of CN^+, $^{13}C^{p+}$ and $^{14}N^{q+}$ ions implanted in copper with a terminal voltage of 400 kV on our Tandetron accelerator. As the CN molecule is broken hitting the surface of copper sample, the projected range of $^{13}C^{14}N^+$ corresponds to average of the ones of ^{13}C at 401 keV and ^{14}N at 432 keV.

Ion species	E (keV)	R_{SRIM} (nm)	R_{exp} (nm)
$^{13}C^{14}N^+$	833	429	440
^{13}C	208	257	280
$^{13}C^+$	608	606	650
$^{13}C^{2+}$	1008	866	910
^{14}N	225	240	260
$^{14}N^+$	625	550	600
$^{14}N^{2+}$	1025	775	820

2. Experimental

2.1. Materials and substrate implantation

The samples were polished polycrystalline copper substrates (12 mm in diameter and 1.5 mm in thickness) which were simultaneously implanted with ^{13}C and ^{14}N atoms using the non-deflected beam line of the 2 MV ALTAÏS[1] accelerator at LARN.[2] In this system, a large variety of CN^+, C^{p+} and N^{q+} (p, q = 0, 1 or 2) cations are produced and co-implanted into the sample with an energy determined by the terminal voltage of the accelerator and their state of charge (Table 1) [16]. During the implantation procedure, the substrate temperature was maintained at 25, 250, 350 or 450 °C and the implantation chamber pressure did not exceed 5×10^{-6} mbar. The current density of the ion beam was approximately 80 μA cm^{-2} and the total fluence was about 10^{18} at. cm^{-2} over an area of 3 mm in diameter.

An implantation of ^{13}C and ^{15}N was performed in order to highlight the presence of nitrogen gas bubbles into the copper sample by mass spectroscopy. The temperature of implantation was fixed at 250 °C. All other parameters of implantation remained unchanged.

2.2. Sample characterisation

The depth distributions of carbon and nitrogen within copper were studied using (d, p) and (d, α) non-resonant nuclear reactions induced on light elements (^{12}C, ^{13}C, ^{14}N and/or ^{15}N) by a 1.05 MeV deuteron beam. The experimental set-up used to perform these measurements was presented in a previous work [17].

XPS depth profile procedures were performed to study the composition and the nature of the carbon nitride compounds synthesised during the ion implantation. One depth profile procedure consists of about 30 cycles of recording the C 1s, N 1s, O 1s and Cu $2p_{3/2}$ peaks followed by etching of the sample. XPS spectra were recorded with a SSX 100 spectrometer system (Surface Science Instrument) equipped with a constant pass energy hemispherical electron analyser. For each cycle, the chemical composition of the sample was measured from the calculated areas of the detected XPS peaks, performing Shirley background subtraction and taking into account sensitivity factors for each line of constituent. The depth profile of the sample is then obtained by converting the etching time into a nanometric depth scale [16]. Moreover, for each cycle, the spectra were referenced to the Cu $2p_{3/2}$ metallic copper line set at binding energy of 932.7 eV. The peaks were fitted using mixed Gaussian–Lorentzian curves (70–30%). Binding state information was then determined from chemical shifts observed on the binding energy scale after the curve fitting of XPS peaks. More details about the experimental set-up and the XPS depth profile procedure were recently published [16].

A mass spectrometer Dycor from Ametek Company was used to confirm the presence of nitrogen gas bubbles assumed by XPS measurements. This spectrometer was able to analyse mass from 1 to 100 amu with a mass resolution of 0.5 amu and a sensitivity of 6×10^{-12} mbar (minimal partial pressure detectable). It was connected to a small analysis chamber which maintained an initial pressure of 6×10^{-7} mbar. To perform the analysis, the N_2 molecules had to be released from the copper matrix by dissolving the sample within a small quantity of iron perchloride acid. The acid was placed into a test tube equipped with a platform allowing us to initially keep the sample apart from the acid. As the vapour pressure of the water contained within the acid is around 20 mbar, we used a leak valve to connect the test tube to the analysis chamber and limit the residual pressure inside the mass spectrometer to 8×10^{-5} mbar. The trend of 16 and 18 amu peaks intensity, related to the vapour of water released by the acid, were then followed using the mass spectrometer. When intensity of these signals became stable, the mass spectrometer switched to follow the trend of 30 amu peak intensity, and the implanted sample was dropped into acid by tapping the test tube. This experiment was performed using a sample implanted with ^{13}C and ^{15}N atoms in order to separate the $^{15}N_2$ signal (mass 30) from the intense signal coming from the $^{12}C^{16}O$ molecules (mass 28) present in the residual pressure of the analysis chamber.

The carbon nitride structures synthesised during the ion implantation were characterised by TEM using a JEOL 3010 (operating at 300 keV) and a CM20 Philips microscopes (operating at 200 kV). EELS measurements were performed on a Philips CM-30-FEG microscope equipped with a post-column GIF200 system. The spectrum was recorded operating the microscope in the diffraction mode with an accelerating voltage of 300 kV and a spectrometer collection angle of 2.5 mrad. Cross-sectional TEM view was required to observe the buried carbon nitride compounds in the copper. This was carried out using a double-beam FIB system consisting of a JEOL 5910 SEM coupled to a Orsay Physics ion column. The 30 keV Ga^+ FIB beam, oriented at 60° with respect to the electron beam, allowed us to very precisely mill specific areas with a minimum damage caused to the area of interest [18]. The cross-sectional preparation of implanted samples was performed step by step. We used first a large beam current (~1 nA) to mill two trenches on either side of the area of interest. Their typical dimensions were 10 μm × 10 μm × 4 μm (length, width and depth), and the space left between them was about 3 μm in order to obtain a slide of the implanted sample of about 10 μm × 3 μm × 4 μm. This slide was then thinned using a succession of smaller beams: 600 pA thinning down to 1 μm; followed by 250 pA to 400–300 nm; and finally 100 pA to 200–100 nm. At this point, the sample was tilted by 45–60° to cut the sides and underside of the thinned slide in order to free it. The slide was then lifted out using a glass rod under an optical microscope (×20 magnification) and placed on a TEM grid with 300 mesh coated with a very thin carbon film, ready for microscopy.

The mechanical properties of the implanted samples were studied using a Hysitron Inc. Triboindenter. The system has a load resolution of 0.1 μN and a displacement resolution of 0.1 nm, which creates indentation curves on the nanometre scale. Experiments were performed using a Berkovich indenter having a face angle of 65.3°. The tip area function was calibrated using fused quartz as reference [19]. Six series of indents were made for each sample: three inside and three outside the implanted area. Each series consisted of 25 indents ranging from 400 μN to 10 mN in 400 μN steps. The indent schedule used was 5 s, 10 s and 5 s for the loading, holding and unloading segment duration, respectively. After each indent, the load–displacement curve was recorded and the tip was moved 10 μm to perform the following indent. For each load–displacement curve, the unloading part was fitted with a power law in order to derive the local stiffness. The hardness and reduced Young's modulus were then calculated using the method described by Oliver and Pharr [19].

3. Results and discussion

In the following section we present first the results obtained by NRA and we compare them to the carbon and nitrogen depth profiles deduced from the XPS measurements. The presence of nitrogen gas bubbles in copper, suggested by this comparison, is then highlighted by mass spectroscopy. The characteristic C–N bonds as a function of depth and temperature of implantation are discussed on the basis of N 1s and C 1s XPS curve fitting. Thereafter, we present the TEM results showing the structure of the carbon nitride compounds, and we finish by determining the mechanical properties of the implanted samples.

3.1. Carbon and nitrogen depth profiles

The experimental spectra recorded by nuclear reaction analysis (not shown here) can be fitted with the SIMNRA code [20]. The target composition used by this software has to be adjusted in order to obtain the best agreement between the experimental and the simulated curves [16]. The carbon (open circles) and nitrogen (open squares) depth profiles, obtained by this method for the sample implanted at 250 °C, are shown in Fig. 1a and b, respectively. A surface contamination of carbon is clearly observed. This contamination is attributed to the carbon build-up phenomenon occurring during the implantation process. It is less significant when the implantation temperature increases. The carbon and nitrogen depth profiles may be decomposed in a combination of Gaussian curves assigned to the different implanted ion species. This decomposition is not represented in Fig. 1, but the positions of each Gaussian curve maximum are reported in Table 1. It can be seen that there is very good agreement between these positions (R_{exp}) and the projected ranges calculated by SRIM2003 (R_{SRIM}) [21], which suggests that carbon and nitrogen diffusions were

[1] Accélérateur Linéaire Tandetron pour l'Analyse et l'Implantation des Solides.
[2] Laboratoire d'Analyses par Réactions Nucléaires.

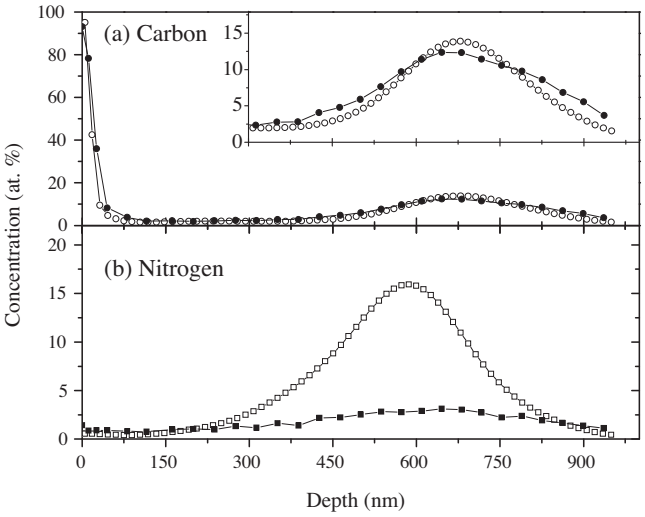

Fig. 1. Concentration depth distributions of carbon and nitrogen calculated from SIMNRA open symbols and CasaXPS (solid symbols) simulations for the copper sample simultaneously implanted with ^{13}C and ^{14}N at 250 °C.

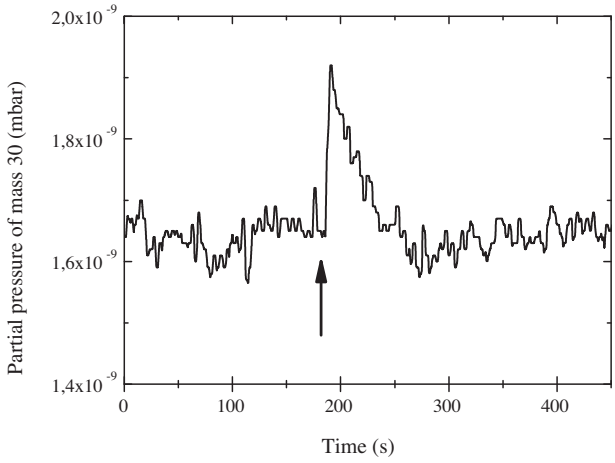

Fig. 2. Time evolution of the 30 amu partial pressure recorded by mass spectroscopy. The arrow indicates when the implanted sample was dropped into the iron perchloride acid.

quite limited during the implantation process. This remains true at all implantation temperatures. Finally, converting the nanometric scale in a 10^{15} at. cm^{-2} scale, the integral of depth profiles allow us to estimate the incorporated carbon and nitrogen atomic densities into copper. The results are presented in Table 2 (D_R – NRA) for each implanted sample. The retained doses evaluated for carbon and nitrogen are very close to the fluence (divergence lower than 10%) regardless of the implantation temperature, which implies that carbon and nitrogen migration and surface release processes did not occur during the implantation.

The carbon (solid circles) and nitrogen (solid squares) depth profiles obtained by XPS for the same sample are presented in Fig. 1a and b, respectively. The agreement between the NRA and XPS carbon depth profiles is very good, even if the XPS one is slightly broader and less intense due to the roughness induced by the etching process. The carbon retained doses deduced from XPS measurements (D_R – XPS) for the different temperature of implantation are reported in Table 2. These values are very close to the initial fluence and the carbon retained doses evaluated by NRA (D_R – NRA). On the other hand, the nitrogen depth profile obtained by XPS is strongly different from the NRA one (Fig. 1b). As reported in Table 2, the nitrogen retained doses, deduced from XPS results for the different implantation temperatures, represent only about 30% of the nitrogen retained doses evaluated by NRA. This strong divergence is explained by assuming that the majority of the implanted nitrogen atoms precipitate into gas bubbles. These bubbles then burst during XPS etching process releasing the N_2 molecules into the chamber before the XPS analysis is performed. The presence of nitrogen gas bubbles inside copper was highlighted by the mass spectroscopy analysis of the sample implanted with ^{13}C and ^{15}N atoms. The evolution of the 30 amu partial pressure as a function of time is shown in Fig. 2. The arrow indicates when the implanted sample was dropped into the acid. A few seconds later, we can clearly observe an abrupt increase of the 30 amu partial pressure which rapidly returns to its initial level. Although qualitative, this result proves the presence of nitrogen gas in the implanted sample.

3.2. Characterisation of chemical bonds

The signature of N_2 molecules can also be observed in the N 1s core level photoelectron spectrum which is shown in Fig. 3a. This spectrum was recorded at 645 nm depth for the sample implanted at 250 °C. According to the literature [22], the rather broad and well separated component N_3 (centred at 404.1 eV, FWMH = 3.6 eV) can be attributed to nitrogen gas molecules. Two other components (N_1 and N_2) can be clearly resolved in this spectrum. The N_1 component (centred at 398.6 eV, FWMH = 1.7 eV) is assigned to the nitriles (–C≡N) and pyridine (C–N=C) type bonds while N_2 (centred at 400.6 eV, FWMH = 1.8 eV) is attributed to sp^2 C–N bonds [23–25]. The N_4 component (centred at 397.2 eV, FWMH = 1.7 eV) may be added in the low energy tail of the N 1s peak. It is assigned to the C_3N_4 structure.

The C 1s core level photoelectron spectrum, acquired on the same sample and at the same depth, is presented in Fig. 3b. The asymmetry of the main peak towards the higher binding energy reveals the presence of C–N and C–O bonds due to the higher electronegativity of nitrogen and oxygen. Nevertheless, contrary to the N 1s spectrum, no component can easily be distinguished. Based on the information resulting from the N 1s and O 1s lines (not shown here), five components have been used to fit the C 1s spectrum. The major component C_0 (centred at 284.4 eV, FWMH = 1.8 eV) is attributed to carbon atoms bonded to carbon

Table 2
Fluence and carbon and nitrogen retained doses evaluated by nuclear reaction analysis (D_R – NRA) and X-ray photoelectron spectroscopy (D_R – XPS) for the samples implanted at 25, 250, 350 and 450 °C.

Temperature of implantation (°C)	Carbon			Nitrogen		
	Fluence (10^{17} at. cm^{-2})	D_R – NRA (10^{17} at. cm^{-2})	D_R – XPS (10^{17} at. cm^{-2})	Fluence (10^{17} at. cm^{-2})	D_R – NRA (10^{17} at. cm^{-2})	D_R – XPS (10^{17} at. cm^{-2})
25	5.0	4.7	4.6	5.0	5.1	1.5
250	5.0	4.9	5.0	5.0	4.6	1.3
350	5.0	4.8	4.7	5.0	4.5	1.2
450	5.0	4.8	4.5	5.0	4.8	1.5

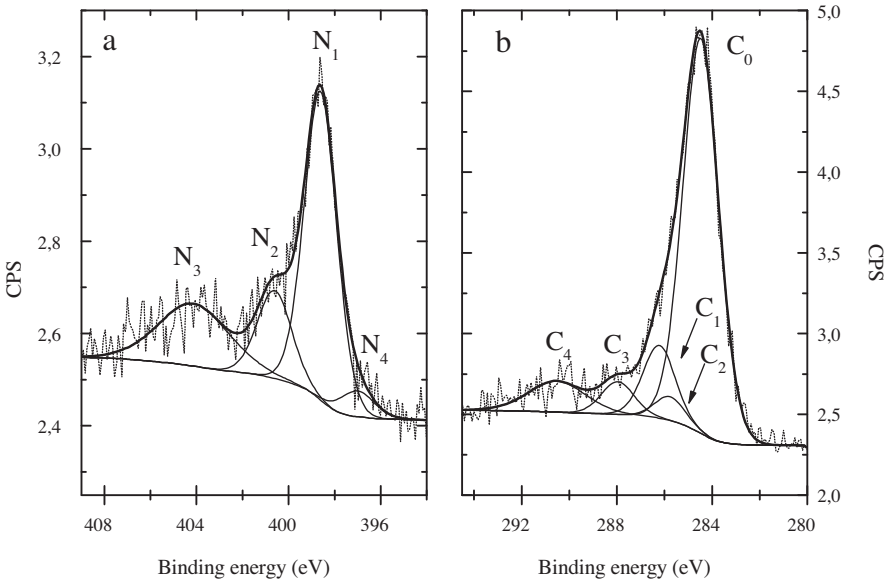

Fig. 3. N 1s (a) and C 1s (b) XPS spectra recorded at a 645 nm depth for the copper sample implanted with ^{13}C and ^{14}N at 250 °C. Experimental data are represented by short dot lines. Solid lines are the results of the curve fitting Gaussian–Lorentzian components and the sum of them.

neighbours, as graphite (sp^2) or amorphous (sp^3) carbon. The C_1 (centred at 286.3 eV, FWMH = 1.6 eV) is assigned to nitriles (–C≡N) and pyridine (C–N=C) type bonds while the C_2 (centred at 285.8 eV, FWMH = 1.5 eV) is attributed to sp^2 C–N bonds [23–26]. In order to be consistent with the N 1s results, the following constraint was imposed on the C_1 and C_2 areas to perform the curve fitting:

$$0.90 \times B(N_i) \leq A(C_i) \leq 1.10 \times B(N_i) \quad \text{for} \quad i = 1 \quad \text{or} \quad 2$$

where $A(C_i)$ is the peak area of component C_i and $B(N_i)$ is the peak area of the component N_i normalised by the sensitivity factor of nitrogen. The C_3 component (centred at 288.0 eV, FWMH = 1.7 eV) is assigned to C–O bonds coming from a slight oxidation of the sample occurring during the etching process. C_4 (centred at 290.5 eV, FWMH = 2.8 eV) is related to the carbon shake up phenomenon [27].

Each cycle of the XPS depth profile was analysed as described above in order to study the evolution of the different carbon nitride compounds (N_1, N_2 or N_4 components) as a function of depth. During this procedure, the position and the FWMH of each component did not change by more than 0.2 eV compared to the values given above. Moreover, whatever the depth analysed, the ratio between the C_3 area and the normalised area of the O 1s peak is always observed to be between 0.85 and 1.15. Besides, the shakeup contribution represents always about 15% of the C_1 peak area. For each cycle of the XPS depth profile, we calculated the ratios between the atomic concentration of each carbon nitride compound (N_1, N_2 or N_4 components) and the total atomic concentration of carbon (sum of C_0, C_1, C_2, C_3 and C_4 components). The mean ratios obtained for the depth between 200 and 900 nm are presented in the third column of Table 3. The first two hundred nanometres were not taken into account in this average due to the very weak intensity of the C 1s and N 1s signals in this area. The rather large standard deviations reported in Table 3 reveal the difficulty in properly performing the exact background fitting of the N 1s and C 1s spectra. This effect is particularly significant for the N_4 component due to its very weak peak intensity.

The mean ratios determined for the samples implanted at 25, 350 and 450 °C are also presented in Table 3. We can observe that the sp^2 and C_3N_4 type bonds are not influenced by the temperature of implantation. About 3.8% of the carbon atoms are bonded to nitrogen in the sp^2 hybridised state while about 1.9% of the carbon atoms are implicated within the C_3N_4 structure, regardless of the implantation temperature. The nitrile (–C≡N) and pyridine (C–N=C) type bonds concerned about 13.5% of the carbon atoms as long as the implantation temperature does not exceed 350 °C, and seems to increase to about 19.5% at 450 °C. The standard deviation on the ratio calculated at 450 °C is nevertheless much larger and its value may thus be overestimated. Consequently, the apparent increase of the nitrile and pyridine type bonds at 450 °C will not be discussed in this work. In summary, the incorporation of nitrogen into the carbon nanostructures remains around 20.7% regardless of the implantation temperature (fifth row of Table 3). The fullerene-like (FL) structure highlighted by TEM (see further) can explain this result. Indeed, the FL structure is generally described as nanoparticles composed of concentric graphitic layers of which the curvature is assured by the presence of pentagonal rings. In addition, total energy calculations show that nitrogen incorporation in graphitic sheets favours the formation of pentagons and thus induces the curvature of the sheets [28]. The FL C_xN_y are however energetically less stable if more than one carbon is substituted in a ring and/or nitrogen is incorporated next to each other, which from geometrical conditions explains the apparent saturation in

Table 3
Mean ratios between the atomic concentration of nitrile and pyridine C–N bonds ($\{N_1\}$), sp^2 C–N bonds ($\{N_2\}$), C_3N_4 structure ($\{N_4\}$) or all C–N bonds together ($\{C\text{–}N\}_{total}$) and the total atomic concentration of carbon ($\{C\}_{total}$). These ratios were evaluated for depth between 200 and 900 nm and for the samples implanted at 25, 250, 350 and 450 °C.

Temperature of implantation	25 °C	250 °C	350 °C	450 °C
$\{N_1\}/\{C\}_{total}$	0.148 ± 0.037	0.126 ± 0.034	0.131 ± 0.035	0.195 ± 0.065
$\{N_2\}/\{C\}_{total}$	0.035 ± 0.007	0.041 ± 0.005	0.037 ± 0.007	0.037 ± 0.006
$\{N_4\}/\{C\}_{total}$	0.022 ± 0.017	0.019 ± 0.016	0.017 ± 0.014	0.019 ± 0.015
$\{C\text{–}N\}_{total}/\{C\}_{total}$	0.205 ± 0.042	0.186 ± 0.039	0.185 ± 0.040	0.251 ± 0.074

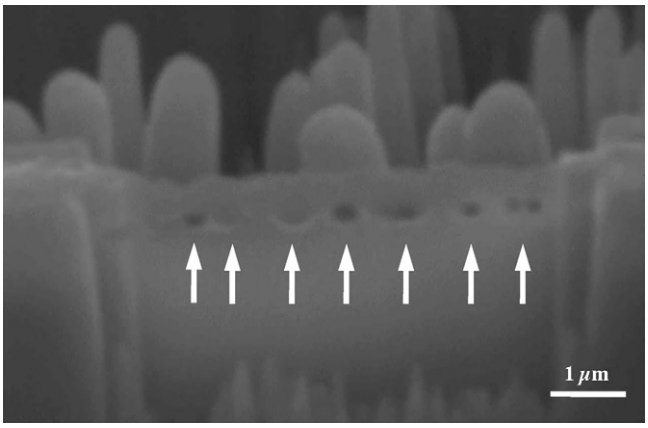

Fig. 4. Lamella of the copper sample implanted at 250 °C, imaged by SEM during the last step of FIB preparation. The arrows point to large empty cavities appearing about 500 nm beneath the sample surface.

maximum nitrogen concentration of approximately 20–25 at.%. Neidhardt et al. confirmed these theoretical predictions by reactive magnetron sputtering [10,29]. In their work, the FL C_xN_y structure was studied as a function of the N_2 fraction in the discharge (varied from 0.16 to 1) and the substrate temperature (varied from 600 °C to −130 °C). Their results show that, whatever the conditions of deposition, the nitrogen content in the FL C_xN_y remains between 18 and 26 at.%, which is in very good agreement with the present work.

3.3. Electron microscopy characterisations

Cross-sectional samples were prepared for the TEM observations. Fig. 4 shows a lamella (∼150 nm thick) imaged by SEM during the FIB preparation of the sample implanted at 250 °C. The arrows point to large empty cavities (up to 200 nm) at approximately 500 nm beneath the surface of the sample. These cavities, attributed to large nitrogen gas bubbles, weaken the copper matrix and make the loss of the top-side of the lamella very difficult to avoid during the lift-out procedure. Only some lamellas were then suitable for the TEM observations.

Typical cross-sectional TEM observation, performed on the sample implanted at 250 °C, is shown in Fig. 5. The top surface of the sample is in the bottom left-hand corner of the picture. Two different nano-objects can be observed: large, bright non-spherical

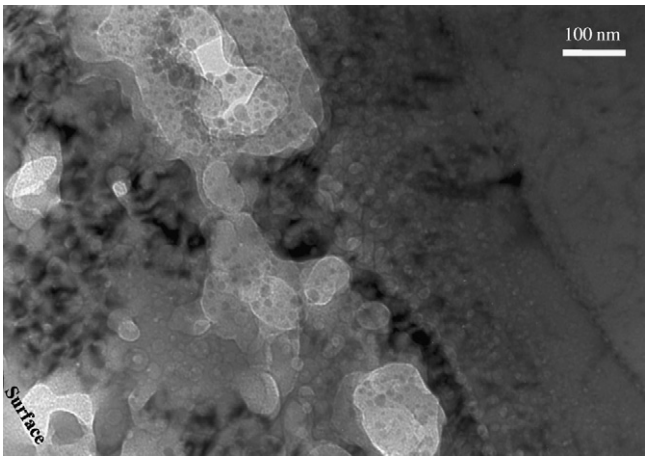

Fig. 5. Cross-sectional TEM observation performed at low magnification on the sample implanted at 250 °C. The surface of the copper sample is in the bottom left-hand corner of the image.

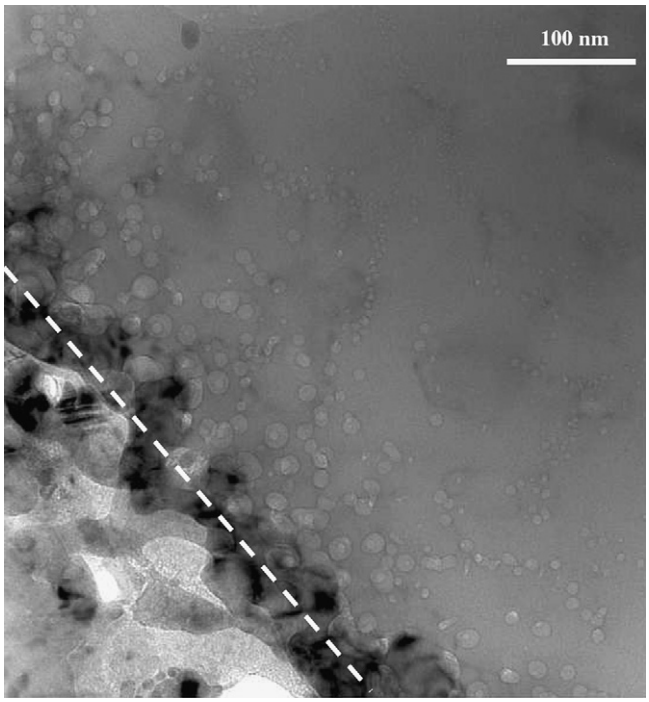

Fig. 6. Cross-sectional TEM observation performed at medium magnification on the sample implanted at 250 °C. Although not visible, the surface of the copper sample is towards the bottom left-hand corner of the image.

cavities and smaller and more spherical nano-capsules. The large cavities are attributed to large nitrogen gas bubbles. Their size ranges from few tens of nanometres to 200 nm and they are mainly concentrated between 400 and 600 nm in depth, which agrees with the NRA and SEM measurements (Figs. 1 and 4). The nano-capsules are assigned to the FL C_xN_y compounds observed by XPS. They spread out from the surface to more than 900 nm in depth with a maximum concentration at around 600 nm. Fig. 6 presents another region of the same sample imaged with a higher magnification. Although not observable, the surface of the sample is again towards the bottom left-hand corner of the picture. The white dotted line corresponds to the maximum in the carbon concentration (∼600 nm depth). The comparison between Fig. 6 and the depth profile of carbon (Fig. 1a) shows the strong correlation between the FL C_xN_y size and the carbon concentration. The biggest FL C_xN_y (∼20 nm) are close to the maximum in the carbon concentration while their size decreases with increase of depth, to become only few nanometres at depth at around 900 nm. The size distribution (not shown here) of the FL C_xN_y deduced from Fig. 6 exhibits a maximum around 12 nm in diameter, which is the typical size of FL structures synthesised by carbon implantation in copper and silver in similar conditions [30–32]. We can also clearly see that the FL C_xN_y are aggregated along slightly more dark lines of which the neighbouring areas are completely free from nano-particles. By comparison with the literature [32], we assume that these lines correspond to the copper grain boundaries which behave like preferential sites for precipitation of the carbon and nitrogen atoms during the implantation process. Finally, the core of FL C_xN_y synthesised in this work seems different from the external shells as observed at medium or high magnification in Figs. 6 and 7, respectively. The cores of these nano-particles appear more illuminated than the external shells, attributed to a lower density.

All these XPS and TEM observations, as well as researches undertaken by Cabioch et al. [30] and Czigany et al. [29], enabled us to work out a growth model for the FL C_xN_y structures synthesised by simultaneous implantation of carbon and nitrogen in copper. This

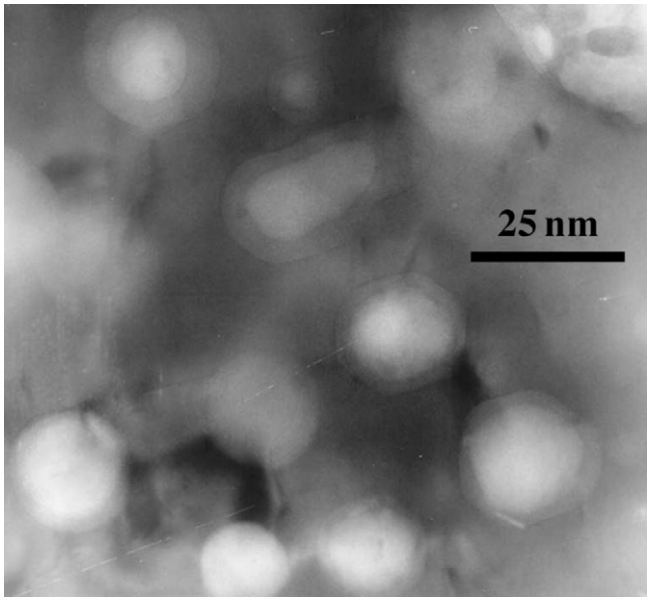

Fig. 7. Cross-sectional TEM observation performed at high magnification on the sample implanted at 250 °C. The area observed is close to the maximum of carbon concentration (~600 nm in depth).

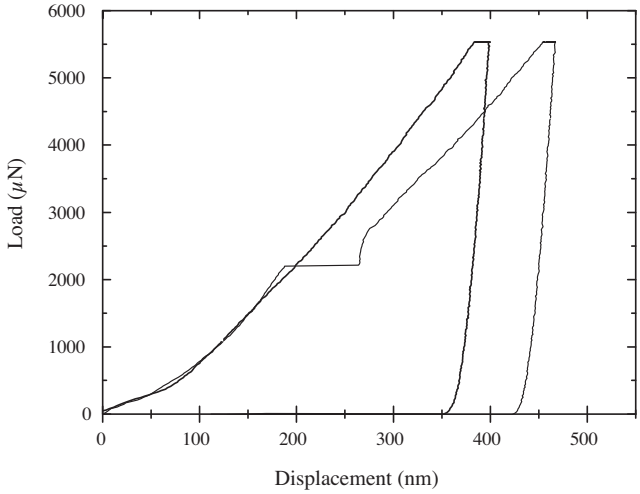

Fig. 8. Nano-indentation load–displacement curves acquired at two different locations inside the irradiated area of the sample implanted at 250 °C. Both measurements were performed with the same indent schedule and maximum load (5600 μN).

model comprises several steps exposed hereafter:

- At the beginning of the implantation process, implanted carbon and nitrogen atoms diffuse towards the grain boundaries driven by the chemical gradient due to the immiscibility of carbon and nitrogen inside the copper host matrix.
- Due to the randomness of diffusion processes, a new incoming atom can meet another atom and chemically bind to it according the one of the following cases:
  - A carbon atom meeting another carbon atom forms sp^2 bond like in graphite.
  - A nitrogen atom meeting another nitrogen atom forms strongly covalent bonded N_2 molecule.
  - A nitrogen atom meeting a carbon atom forms C–N chemical bond, which again can occur in various ways:
    - Nitrogen and carbon atoms form sp^3 bond as in the C_3N_4 structure, which is the less likely case according to XPS measurements (~2% as shown in Table 3).
    - Nitrogen and carbon atoms form nitrile and pyridine or sp^2 C–N bonds (~18% as shown in Table 3).Any case, as demonstrated by total energy calculations [28], the nitrogen incorporation in the graphitic compounds will induce the curvature and then the formation of FL C_xN_y structures.
- New incoming atoms then precipitate and form one of the chemical bonds depicted above, contributing to the growth of N_2 bubbles or FL C_xN_y structures.

This growth model explains the formation of FL C_xN_y structures and N_2 bubbles observed in this work. In addition, NRA depth profiles (Fig. 1) showed that nitrogen concentration is always higher than 20% of the carbon concentration, regardless of depth and temperature of implantation. That means that FL C_xN_y structures are forming in presence of N_2 molecules since, for a same depth location, all implanted nitrogen atoms cannot be integrated within FL C_xN_y structures for which the nitrogen content is limited at about 20 at.% [10,28,29]. That suggests that N_2 molecules are formed before that first shell of FL C_xN_y structures is completed. Some of these molecules can consequently be surrounded by the FL C_xN_y structures, which may explain the lower density of the FL C_xN_y structures as observed by TEM. This assumption is supported by EELS measurements (not shown here) acquired on some well isolated FL C_xN_y. The nitrogen content of the FL C_xN_y deduced from EELS measurements was measured to be about 30 at.%, whereas XPS yielded only about 20 at.% (Table 3). This difference is attributed to the N_2 molecules (not taken into account in Table 3) that could constitute the core of FL C_xN_y. This growth model agrees with all measurements presented in this work.

No significant modifications of the FL C_xN_y size and structure have been observed as a function of the implantation temperature, which differs from the results obtained by carbon implantation in copper [30]. Indeed, this reference shows that the size of the carbon nano-structures is increased and its crystallinity is strongly enhanced when the temperature is varied from 400 to 1000 °C. Moreover, no FL structures are obtained for implantation temperatures lower than 600 °C. In contrast, the present work shows that FL C_xN_y structures can be formed at implantation temperatures ranging from 25 to 450 °C. This confirms that the incorporation of nitrogen into carbon layers favours the formation of FL structures. The nano-compounds synthesised by co-implantation of carbon and nitrogen in copper remain nevertheless amorphous regardless the implantation temperature.

3.4. Tribological measurements

Fig. 8 shows two load–displacement curves acquired at two different locations inside the irradiated area of the sample implanted at 250 °C. Although recorded for exactly the same indent schedule and maximal load, only one load–displacement curve presents a discontinuity in the loading part. This phenomenon occurred for about 40% of the indents performed inside the implanted areas whereas it was observed for only about 5% outside these areas. Moreover, the discontinuities always appeared between 200 and 500 nm in displacement. We attributed these discontinuities to a movement of the copper matrix which is weakened by the large nitrogen gas bubbles highlighted before. As this phenomenon strongly affects the hardness deduced from the load–displacement curve, we decided not to take into account these indents to determine the mechanical properties of the implanted samples. The mean hardness and Young's modulus evaluated for the copper substrate and the implanted area are

Table 4
Mean hardness and Young's modulus values for the substrate and the irradiated area of the samples implanted at 25, 250, 350 or 450 °C.

Temperature of implantation	Hardness (GPa)		Young's modulus (GPa)	
	Substrate	Implanted area	Substrate	Implanted area
25 °C	0.97 ± 0.15	1.23 ± 0.19	106.4 ± 6.5	95.6 ± 8.8
250 °C	1.00 ± 0.14	1.21 ± 0.20	112.6 ± 7.3	104.3 ± 5.8
350 °C	0.93 ± 0.09	1.17 ± 0.18	110.2 ± 7.1	98.5 ± 8.5
450 °C	0.98 ± 0.08	1.19 ± 0.10	104.0 ± 6.1	97.0 ± 7.5

reported in Table 4 for the samples implanted at 25, 250, 350 and 450 °C.

Irrespective of the implantation temperatures, the hardness and the reduced Young's modulus of the copper substrate are around 0.97 GPa and 108 GPa, respectively (Table 4). These results correspond to the values generally observed in the literature [33,34]. As suggested by the XPS and TEM results, no significant variation of the mechanical properties irradiated area is observed with increase in the implantation temperature. The hardness remains close to 1.20 GPa while the Young's modulus is about 99 GPa, irrespective of the temperature. The co-implantation of carbon and nitrogen has thus the ambiguity of enhancing the copper hardness by about 25% while weakening some areas of the sample. Moreover, the hardness achieved in this work remains much lower than that obtained by physical vapour deposition of C_xN_y films (7–18 GPa) [35].

4. Conclusion

Simultaneous implantation of ^{13}C and ^{14}N in copper were performed in order to synthesise carbon nitride compounds. The total fluence was fixed at 10^{18} at. cm^{-2} and the substrate temperature was maintained at 25, 250, 350 or 450 °C. The retained doses and depth profiles of carbon and nitrogen were determined by NRA. The formation of FL C_xN_y compounds during the implantation process was highlighted by XPS and TEM. At least three different configurations of C–N types bond were formed: the nitrile (–C≡N) and pyridine (C–N=C) type bonds; the sp^2 C–N bonds; and a very small contribution of C_3N_4 structure. We have nevertheless shown that most of the nitrogen precipitates into large gas bubbles. Only about 20% of the implanted ^{14}N atoms are contained in the FL C_xN_y structures, whatever the temperature of implantation. Based on our TEM results, the total energy calculations and the works of Cabioch et al., we have proposed a growth model in which the core of FL C_xN_y nano-particles is composed of N_2 molecules. Finally, the nano-indentation measurements have shown that the mechanical properties of copper can be slightly enhanced by ^{13}C and ^{14}N co-implantation. The hardness achieved remains nevertheless much lower than that obtained by physical vapour deposition of C_xN_y films.

Acknowledgements

The authors thank Prof. G. Van Tendeloo for the use of microscopes of EMAT laboratory (University of Antwerp, Belgium). The authors are grateful to T. Cabioch, from the University of Poitiers (France), for helpful discussions on the growth model of the C_xN_y structures. The nano-indentation measurements were carried out at the University of Brussels (ULB, Belgium) with the support of Dr. J. Dille. J.-F. Colomer is supported by the FRS-FNRS (Belgium) as Research Associate.

References

[1] A.Y. Liu, M.L. Cohen, Phys. Rev. B 41 (1990) 10727.
[2] K.M. Yu, M.L. Cohen, E.E. Haller, W.L. Hansen, A.Y. Liu, I.C. Wu, Phys. Rev. B 49 (1994) 5034.
[3] L. Maya, D.R. Cole, E.W. Hagaman, J. Am. Ceram. Soc. 74 (1991) 1686.
[4] C.M. Niu, Y.Z. Lu, C.M. Lieber, Science 261 (1993) 334.
[5] E. Gyorgy, V. Nelea, I.N. Mihailescu, A. Perrone, H. Pelletier, A. Cornet, S. Ganatsios, J. Werckmann, Thin Solid Films 388 (2001) 93.
[6] A. Hoffman, I. Gouzman, R. Brener, Appl. Phys. Lett. 64 (1994) 845.
[7] E.A. Romanovsky, O.V. Bespalova, A.M. Borisov, N.G. Goryaga, V.S. Kulikauskas, V.G. Sukharev, V.V. Zatekin, Nucl. Instrum. Methods B 139 (1998) 355.
[8] J. Jagielski, N. Moncoffre, P. Delichere, G. Marest, J. Mater. Sci. 34 (1999) 2949.
[9] N. Hellgren, M.P. Johansson, E. Broitman, L. Hultman, J.E. Sundgren, Phys. Rev. B 59 (1999) 5162.
[10] J. Neidhardt, H. Hogberg, L. Hultman, Thin Solid Films 478 (2005) 34.
[11] P. Hammer, W. Gissler, Diamond Relat. Mater. 5 (1996) 1152.
[12] R. Kaltofen, T. Sebald, G. Weise, Thin Solid Films 308 (1997) 118.
[13] A. Badzian, T. Badzian, R. Roy, W. Drawl, Thin Solid Films 354 (1999) 148.
[14] C.W. Allen, M. Song, K. Furuya, R.C. Birtcher, S.E. Donnelly, K. Mitsuishi, J. Electron Microsc. 48 (1999) 1025.
[15] B. Deconninck, F. Bodart, Nucl. Instrum. Methods B 137 (1998) 410.
[16] J.L. Colaux, P. Louette, G. Terwagne, Nucl. Instrum. Methods B 267 (2009) 1299.
[17] T. Thome, J.L. Colaux, G. Terwagne, Nucl. Instrum. Methods B 249 (2006) 377.
[18] L.A. Giannuzzi, F.A. Stevie, Micron 30 (1999) 197.
[19] W.C. Oliver, G.M. Pharr, J. Mater. Res. 7 (1992) 1564.
[20] M. Mayer, SIMNRA, a simulation program for the analysis of NRA, RBS and ERDA, in: J.L. Duggan, I.L. Morgan (Eds.), Proceedings of the 15th International Conference on the Application of Accelerators in Research and Industry, American Institute of Physics, University of North Texas, TX, USA, 1998, p. 541.
[21] J.F. Ziegler, Nucl. Instrum. Methods B 219–220 (2004) 1027.
[22] A. Nilsson, O. Bjorneholm, H. Tillborg, B. Hernnas, R.J. Guest, A. Sandell, R.E. Palmer, N. Martensson, Surf. Sci. 287 (1993) 758.
[23] N. Hellgren, J.H. Guo, Y. Luo, C. Sathe, A. Agui, S. Kashtanov, J. Nordgren, H. Agren, J.E. Sundgren, Thin Solid Films 471 (2005) 19.
[24] B. Angleraud, N. Mubumbila, P.Y. Tessier, V. Fernandez, G. Turban, Diamond Relat. Mater. 10 (2001) 1142.
[25] T. Ujvári, A. Kolitsch, A. Toth, M. Mohai, I. Bertoti, Diamond Relat. Mater. 11 (2002) 1149.
[26] C. Palacio, C. Gomez-Aleixandre, D. Diaz, M.M. Garcia, Vacuum 48 (1997) 709.
[27] J.A. Leiro, M.H. Heinonen, T. Laiho, I.G. Batirev, J. Electron Spectrosc. Relat. Phenom. 128 (2003) 205.
[28] S. Stafstrom, Appl. Phys. Lett. 77 (2000) 3941.
[29] Z. Czigany, I.F. Brunell, J. Neidhardt, L. Hultman, K. Suenaga, Appl. Phys. Lett. 79 (2001) 2639.
[30] T. Cabioch, M. Jaouen, E. Thune, P. Guerin, C. Fayoux, M.F. Denanot, Surf. Coat. Technol. 128 (2000) 43.
[31] T. Cabioch, E. Thune, M. Jaouen, Chem. Phys. Lett. 320 (2000) 202.
[32] E. Thune, T. Cabioch, P. Guerin, M.F. Denanot, M. Jaouen, Mater. Lett. 54 (2002) 222.
[33] T.H. Fang, W.J. Chang, Microelectron. Eng. 65 (2003) 231.
[34] L.M. Qian, M. Li, Z.R. Zhou, H. Yang, X.Y. Shi, Surf. Coat. Technol. 195 (2005) 264.
[35] J. Neidhardt, Z. Czigany, I.F. Brunell, L. Hultman, J. Appl. Phys. 93 (2003) 3002.